High pressure elasticity of $FeCO_3$-$MgCO_3$ carbonates

Michal Stekiel[a,*], Tra Nguyen-Thanh[b], Stella Chariton[c], Catherine McCammon[c], Alexei Bosak[b], Wolfgang Morgenroth[a], Victor Milman[d], Keith Refson[e,f], Björn Winkler[a]

[a] *Institute of Geosciences, Goethe Universität, Altenhöferallee 1, 60438 Frankfurt am Main, Germany*
[b] *ESRF The European Synchrotron, 71 Avenue des Martyrs, Grenoble F-38000, France*
[c] *Bayerisches Geoinstitut, Universität Bayreuth, 95440 Bayreuth, Germany*
[d] *Dassault Systemes BIOVIA, 334 Science Park, Cambridge, CB4 0WN, UK*
[e] *Department of Physics, Royal Holloway University of London, Egham, Surrey TW20 0EX, UK*
[f] *ISIS Facility, Science and Technology Facilities Council, Rutherford Appleton Laboratory, Didcot OX11 0QX, UK*

Abstract

We have determined the elastic stiffness moduli of $FeCO_3$ across the spin transition up to 60 GPa by inelastic X-ray scattering and density functional theory calculations. We have derived functions describing the dependence of the components of the elastic tensor of $Mg_{1-x}Fe_xCO_3$ solid solutions on pressure and concluded that there is a linear dependence of the C_{11}, C_{33}, C_{44} and C_{14} moduli on the composition parameter x. The elastic tensors were employed to calculate the sound velocities and velocity anisotropies of $Mg_{1-x}Fe_xCO_3$. These results allow an assessment of the potential seismic signature of deep mantle carbonates.

Keywords: elastic tensor, siderite, magnesite, high pressure, IXS, DFT

1. Introduction

Carbonates play a significant role in the deep carbon cycle of the Earth. They can be transported to the interior of the Earth in subducting slabs, thus potentially contributing to the deep carbon storage in the lower mantle [1]. The most abundant carbonates at shallow depths are calcite/aragonite, $CaCO_3$,

*Corresponding author
Email address: stekiel@kristall.uni-frankfurt.de (Michal Stekiel)

dolomite, $CaMg(CO_3)_2$ and magnesite, $MgCO_3$ [2, 3]. However, during subduction, calcium rich carbonates react with silicate minerals forming iron bearing magnesite $Mg_{1-x}Fe_xCO_3$ [4, 5, 6] which is stable at lower mantle conditions [7, 8, 9]. Knowledge of the elastic properties of $Mg_{1-x}Fe_xCO_3$ carbonates at Earth's mantle conditions is thus important for understanding the deep carbon cycle and is a prerequisite for the prediction of the seismic signature, that would be indicative for carbonates in the mantle.

At ambient temperature and up to 60 GPa both siderite, $FeCO_3$, and magnesite, $MgCO_3$, crystallize in space group $R\bar{3}c$, with octahedrally coordinated cations and planar CO_3 groups [10, 11]. Such a symmetry results in 6 independent C_{ij} moduli: C_{11}, C_{33}, C_{44}, C_{12}, C_{13} and C_{14}. At 45 GPa $FeCO_3$ undergoes a spin transition associated with a 10 % decrease of the unit cell volume [12, 11]. The bulk modulus increases by 18 % across the spin transition from 317 GPa to 373 GPa [11, 13]. Different studies on $Mg_{1-x}Fe_xCO_3$ carbonates reporting the spin transition pressure [13, 14, 15, 16, 17, 18] show that it lies within the region of 40-47 GPa. There is an ongoing discussion on whether this transition is "sharp", i.e. takes place over an interval of 2 GPa [17], or "gradual", i.e. takes place over an interval of 7 GPa [16].

Our knowledge of the pressure dependence of the elastic stiffness tensor of carbonates is currently very limited. Yang et al. (2014) [19] measured the full elastic stiffness tensor of $MgCO_3$ up to 14 GPa at ambient temperature and additionally up to 750 K at ambient pressure by Brillouin scattering in a diamond anvil cell. They reported that the elastic stiffness moduli of $MgCO_3$ increase linearly with pressure and decrease linearly with temperature. Fu et al. (2017) [18] measured the full elastic stiffness tensor of $Mg_{0.35}Fe_{0.65}CO_3$ up to 70 GPa at ambient temperature by Brillouin light scattering and impulsive stimulated light scattering in a diamond-anvil cell. They observed a drastic softening of the C_{11}, C_{33}, C_{12}, C_{13} moduli and stiffening of C_{44} and C_{14} moduli across the spin transition in the mixed-spin state. Outside the region of the spin transition they observed a linear increase of all elastic moduli with pressure. Sanchez-Valle et al.(2011) [20] measured the elastic tensor of $Mg_{1-x}Fe_xCO_3$ for

four different compositions at ambient conditions and concluded that, within the resolution of their data, all elastic stiffness moduli follow linear trends upon substitution of Fe for Mg.

Previous high pressure DFT calculations on $FeCO_3$ [21, 22] report the pressure dependence of the bulk modulus without deriving the full elastic tensor. Shi et al. [21] calculated the spin transition pressure of $FeCO_3$ to be at 28 GPa based on GGA+U calculations. They report an abrupt increase of bulk modulus at the spin transition from 218 GPa to 261 GPa. Hence, their values are in only moderate agreement with Lavina et al. (2009) [11]. Hsu and Huang (2016) [22] investigated $Mg_{1-x}Fe_xCO_3$ carbonates with an iron concentration in a range of x = 0.125-1 employing LDA+U_{sc} calculations. They concluded that the spin transition occurs in the region of 45-50 GPa regardless of the iron concentration. They also calculated the pressure and temperature dependence of the bulk modulus of $Mg_{1-x}Fe_xCO_3$ carbonates taking into account the mixed-spin state. They predict a drastic softening of the bulk modulus along the spin transition which was confirmed experimentally in the case of $Mg_{0.35}Fe_{0.65}CO_3$ [23, 18].

In order to quantify the change in the elasticity of pure $FeCO_3$ across the spin transition we performed an inelastic X-ray scattering (IXS) experiment and complementary DFT calculations to determine the full elastic stiffness tensor. We have investigated the reliability of our computational approach by computing the pressure dependence of the elastic stiffness tensor of $MgCO_3$, and by comparing our results with published data [19, 20, 24, 25]. A combination of all experimental and theoretical data allows us to interpolate the elastic properties of $Mg_{1-x}Fe_xCO_3$ for any composition and pressure up to 60 GPa. From this data we can obtain sound velocities and velocity anisotropies of lower mantle $Mg_{1-x}Fe_xCO_3$ carbonates, which then can be employed in mineral physics models.

2. Experimental methods

Single crystals of $FeCO_3$ were synthesized by following the method developed by French (1971) [26] and Cerantola et al. (2016) [16]. We have tested the quality of the crystals on an Xcalibur single crystal diffractometer or by synchrotron radiation. Crystals of highest quality were chosen for high pressure IXS experiments, their dimensions were 80 × 50 × 22 μm (S18), 35 × 30 × 15 μm (S15) and 25 × 25 × 10 μm (A1). Crystals S18 and S15 were loaded into Boehler-Almax type diamond anvil cells with 350 μm and 300 μm diamond culet size, respectively, and rhenium gaskets with initial hole dimensions 160 × 55 μm (diameter × thickness) and 110 × 40 μm, respectively, with Ne as pressure transmitting medium. Crystal A1 was loaded into a symmetric diamond anvil cell with bevelled diamonds with diameters of 250 μm, a rhenium gasket with initial dimensions 140 × 60 μm and He as pressure medium. Crystal S18 was measured at 2 GPa and 28 GPa, S15 at 15 GPa and A1 at 55 GPa. The pressure was measured before and after IXS measurements at each pressure point. Crystal quality degraded significantly with increasing pressure as indicated by the increase of intensity of the elastic line, see Fig. 1.

IXS measurements were performed at the ID28 beamline of the ESRF. The spectrometer was operating at 17.794 keV incident photon energy providing an instrumental energy resolution of 3 meV. The X-ray beam was focused using KB mirrors to a spot size of 20 × 30 μm. At each pressure point energy scans were performed along the Γ-T direction, around convenient Bragg reflections (see supplementary materials). At 55 GPa measurements along other directions were performed in addition. Before each IXS scan the UB matrix of the crystal was refined, to determine the exact orientation of the crystal and measure the lattice parameters used to determine the density of the sample.

Linear dispersion relations were fitted to the measured data in the vicinity of the Γ point, to obtain the sound velocities. Velocities of the longitudinal phonons were used to determine the C_{33} modulus, and velocities of the transverse phonons were employed to determine the C_{44} modulus by solving the

Christoffel equation [27]. Velocities obtained from additional measurements at 55 GPa were compared with calculated values.

3. Computational details

Spin-polarized density functional theory calculations were performed with commercial and academic versions of the CASTEP program [28] using the generalized gradient approximation formalized by Perdew, Burke & Ernzerhof [29] (PBE) with a plane wave basis set and ultrasoft pseudopotentials from the CASTEP 8.0 database. The maximum cutoff energy of the plane waves was 750 eV. A 12 × 12 × 12 Monkhorst-Pack grid [30] was employed for sampling of the reciprocal space corresponding to a k-point separation of less than ~ 0.022 $Å^{-1}$.

A Hubbard U of 4 eV was employed for the Fe d-electrons. Additional calculations showed that a variation of U by 10 % had only a negligible influence on the elastic stiffness moduli. The calculations were considered to be converged once the maximal residual force acting on an atom was <0.01 eV/Å, the residual stress was <0.02 GPa, and the maximal energy change was $<5 \cdot 10^{-6}$ eV/atom. For the calculations of stress-strain relations two strain patterns were employed. The maximum strain amplitude was 0.003.

The calculations were done in 10 GPa pressure steps for both $MgCO_3$ and $FeCO_3$. In case of $FeCO_3$ we performed the calculation in pure spin state, i.e. in high-spin state from 0 to 40 GPa inclusive, and in low-spin from 40 to 60 GPa inclusive.

4. Results and discussion

4.1. IXS, high pressure elasticity of $FeCO_3$ and $MgCO_3$

Representative high-pressure IXS spectra of $FeCO_3$ are shown in Fig. 1. The velocities derived from low-q phonon dispersion relations of LA and TA branches measured along c* direction were used to determine the C_{33} and C_{44} moduli of the elastic tensor of $FeCO_3$, as shown in Fig. 2. We have performed

complementary DFT calculations to determine the full elastic tensor and compared the results to our data (Fig. 2). Velocities obtained from additional measurements at 55 GPa are compared with calculated values in Fig. 3.

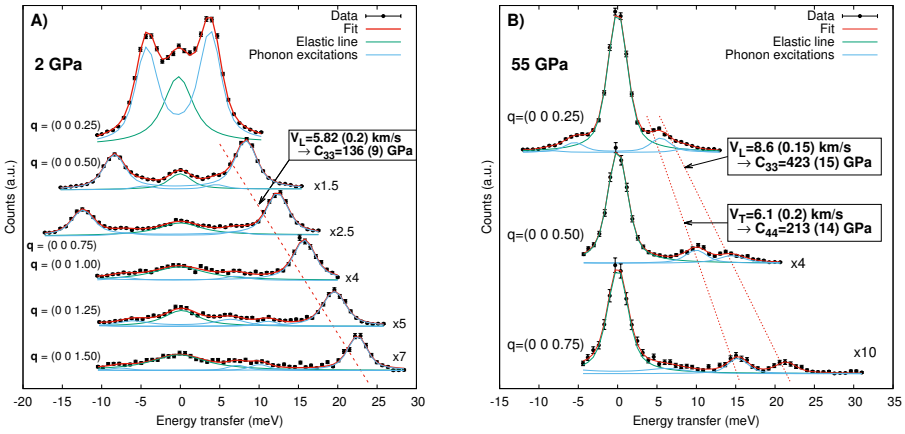

Figure 1: IXS spectra (black points with error bars) of $FeCO_3$ measured at 2 GPa (A) and 55 GPa (B) along with fitted spectra (red lines) that are a combination of phonon excitations (blue lines) and elastic line (green lines). At 2 GPa spectra were measured around the (0 0 12) reflection, and at 55 GPa around the (0 1 -4) reflection. Linear dispersion relations were fitted to determine sound velocities (red dashed lines) and elastic stiffness moduli (see text). "×N" denotes the magnification of the respective spectrum.

The experimental values of C_{33} and C_{44} moduli of high-spin $FeCO_3$ are in good agreement with the results of our calculations. The excellent correspondence between calculated and measured elastic moduli is almost certainly fortuitous as DFT-calculated elastic moduli are typically accurate to a few percent. At ambient pressure the calculated values of C_{12} and C_{13} are lower than the experimental values by 28% and 23%, respectively, other moduli are the same within the given error. We see a linear stiffening of all C_{ij} moduli with pressure, up to the transition pressure. After the spin transition all C_{ij} moduli stiffen abruptly with the exception of C_{12} which in the low spin phase has similar values to the ones extrapolated from the high-spin state. In the low-spin state all C_{ij} moduli stiffen linearly with pressure.

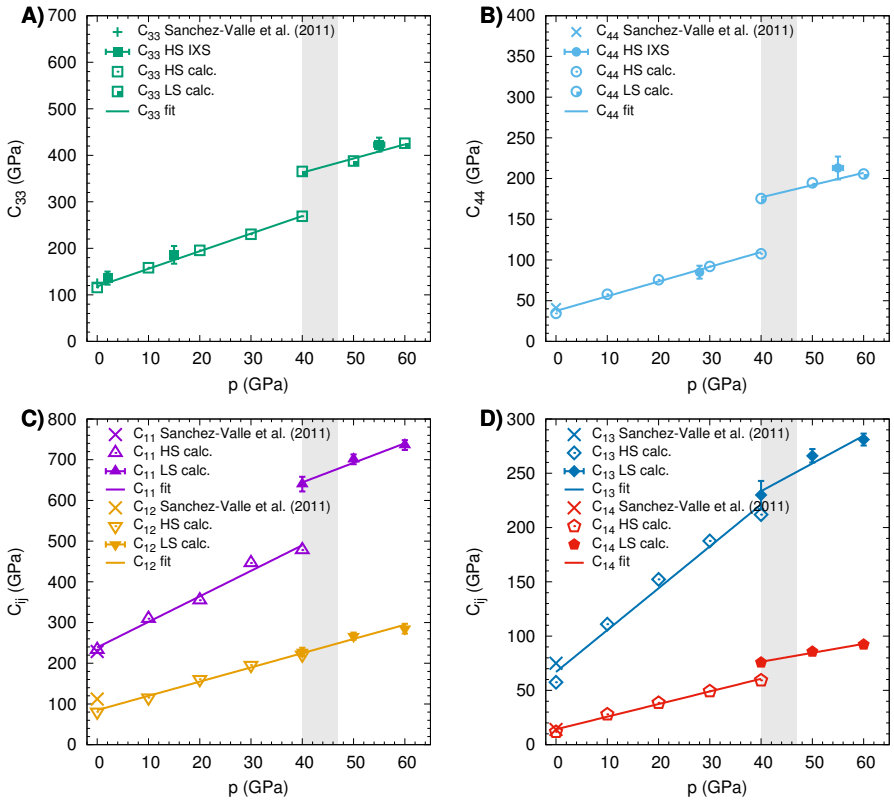

Figure 2: C_{33} (panel A) and C_{44} (B) elastic stiffness moduli of $FeCO_3$ measured by IXS (full symbols) compared with calculated values (empty symbols: high-spin siderite, partially empty: low-spin siderite). Calculated values of C_{11}, C_{12} moduli (C) and C_{13}, C_{14} moduli (D) are indicated by empty symbols (high-spin $FeCO_3$), and full symbols (low-spin $FeCO_3$). "×" denotes the values measured by Sanchez-Valle et al. (2011) [20] at ambient pressure. Solid lines are fits to the calculated values. Shaded area indicates the pressure range of the spin transition [13, 15, 16, 17]. If not shown, errors are smaller than the symbol size.

Comparison between our results on $FeCO_3$ and the results of Fu et al. (2017) [18] on $Mg_{0.35}Fe_{0.65}CO_3$ show the same behavior of the elastic stiffness moduli out of the mixed-spin phase region. All elastic stiffness moduli of the low spin phase stiffen with respect to the extrapolated values of the high spin phase, apart from C_{12}. In the experiment we could not observe a softening of C_{11}, C_{33}, C_{12}, and C_{13} moduli across the spin transition in the mixed-spin state as

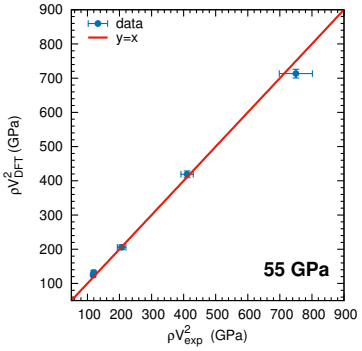

Figure 3: Comparison between sound velocities of $FeCO_3$ measured by IXS at 55 GPa (for details see supplementary materials) and calculated velocities. The value of ρV^2 is proportional to the elastic stiffness moduli.

reported by Fu et al. [18], as the steps with which we increased the pressure were too large. Our calculations also do not reproduce the softening, as they were performed for the pure-spin state of iron.

We have calculated the elastic stiffness tensor of $MgCO_3$ up to 60 GPa, the results are shown in Fig. 4. The calculated values are in good agreement with experiments [19], except for the C_{12} modulus, where our calculations predict a value that is systematically lower by 21%. Experimental data [19] show that all C_{ij} moduli of $MgCO_3$ depend linearly on pressure up to 14 GPa. Our calculations show that C_{33}, C_{12} and C_{13} follow a linear trend even up to 60 GPa, while C_{11}, C_{44} and C_{14} behave non-linearly above 20 GPa. At 60 GPa, for example, the calculated value of C_{11} is smaller by 156 GPa than would be expected from the linear extrapolation.

4.2. High pressure elasticity of $Mg_{1-x}Fe_xCO_3$

In order to investigate the influence of composition on the elastic properties of $Mg_{1-x}Fe_xCO_3$ at high pressures we have compared the elastic tensors calculated in this study with the ones available in the literature, see Fig 5. In the investigated pressure range we observe a linear dependence of C_{11}, C_{33}, C_{44}, C_{13} and C_{14} moduli on the Fe content. Up to the spin transition C_{12} and C_{13}

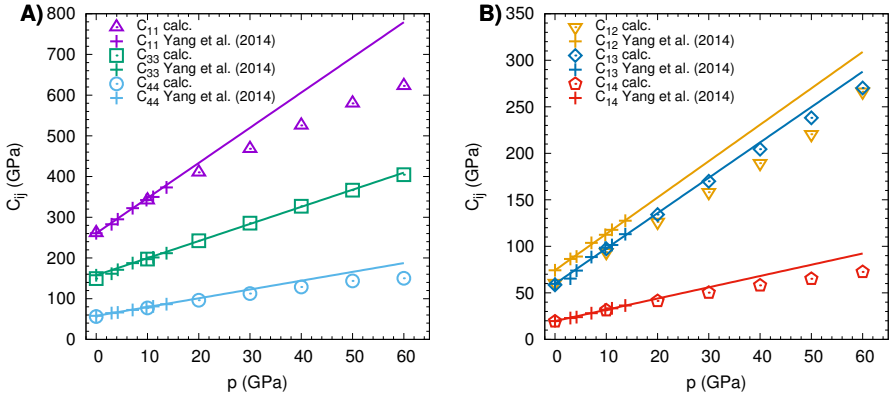

Figure 4: Calculated elastic stiffness moduli of $MgCO_3$ (open symbols) compared to experimental data ("+") [19]. Solid lines are fits to the experimental data. Statistical and fitting errors are smaller than the symbol size.

moduli increase with increasing Fe content, in contrast to the other moduli. After the spin transition all C_{ij} moduli stiffen with increasing Fe content.

4.3. Discussion

The elastic tensors of $Mg_{1-x}Fe_xCO_3$ were employed to calculate the sound velocities and velocity anisotropies, as shown in Fig. 6. The anisotropies were defined as: $AV_i = 2\ (AV_i^{max}\text{-}AV_i^{min})\ /\ (AV_i^{max}+AV_i^{min})$, following Mainprice (2000) [31]. In the whole investigated pressure region the sound velocities of $Mg_{1-x}Fe_xCO_3$ decrease with increasing Fe content. An increase of both compressional (V_p) and shear (V_s) velocities is observed after the spin transition. A detailed analysis shows that the relative change of the sound velocity $[(V_i^{LS} - V_i^{HS})\ /\ V_i^{HS}]$ over the spin transition scales linearly with Fe content. After the spin transition V_p of $FeCO_3$ increases by 11% and V_s by 28%. In the case of $Mg_{0.85}Fe_{0.15}CO_3$, a proposed deep mantle carbonate [32], V_p increases by 2% and V_s by 5%.

The anisotropy of sound velocities increases with increased Fe content, in contrast to the sound velocities. The compressional wave anisotropy increases up to the spin transition and decreases afterwards. The shear wave anisotropy drops

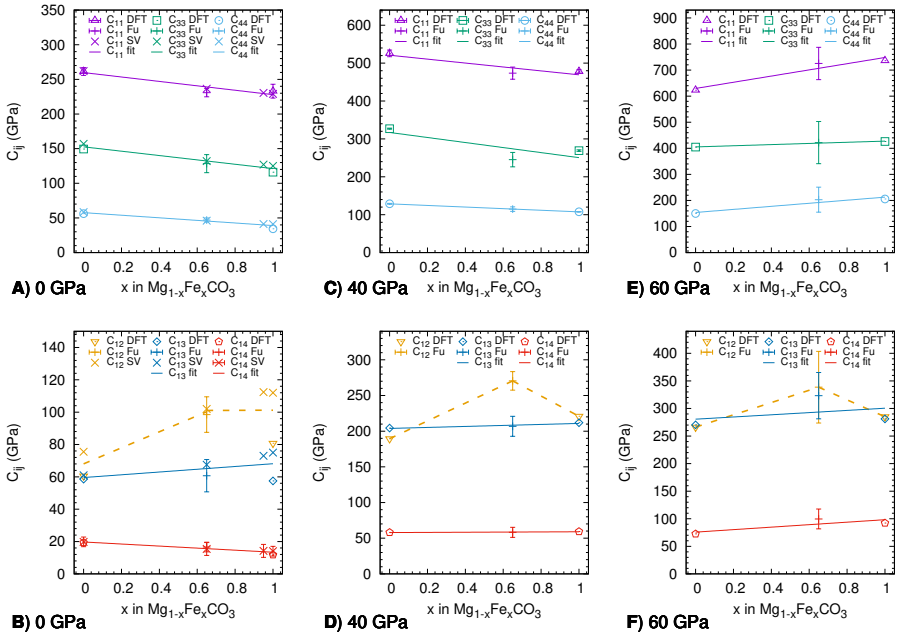

Figure 5: Calculated (this study) and experimental (Fu [18], SV [20]) values of the elastic tensor components of $Mg_{1-x}Fe_xCO_3$ at ambient pressure (panel A, B), 40 GPa (C, D) and 60 GPa (E, F). Top row: diagonal coefficients, bottom row: off-diagonal coefficients. Solid lines are fits to the data, while dashed lines are guides for the eye. In panels C, D the calculated C_{ij} moduli of high-spin $FeCO_3$ are shown. The non-monotonic behavior of C_{12} is due to the systematical difference between calculations and experiment (see text), and C_{13} at 60 GPa is monotonic within experimental error.

after the spin transition by 24% for $FeCO_3$ and less than 1% for $Mg_{0.85}Fe_{0.15}CO_3$. Beyond the region of the spin transition it shows linear behavior.

Our results are consistent with discussions presented by Sanchez-Valle et al. (2011) [20] and Yang et al. (2014) [19]. They did not, however, discuss the influence of the spin transition on the detectability of deep mantle carbonates. Fu et al. (2017) [18] were the first to investigate the sound velocities across the spin transition. Based on their study of $Mg_{0.35}Fe_{0.65}CO_3$ they concluded that V_p would decrease by 10% decrease in a potential deep mantle carbonate, when comparing the minimum velocity in the mixed-spin phase to the one in the high-

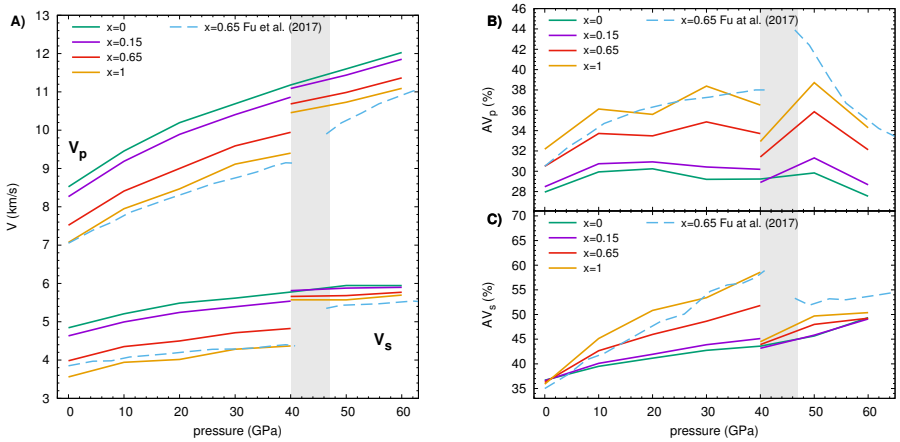

Figure 6: Calculated (solid lines) and experimental (dashed line) [18] sound velocities (panel A) and velocity anisotropies of compressional (B) and shear (C) waves of $Mg_{1-x}Fe_xCO_3$ across the spin transition. The green solid line represents data on $MgCO_3$, the purple solid line on the potential deep mantle carbonate, $Mg_{0.85}Fe_{0.15}CO_3$, the red solid line on $Mg_{0.35}Fe_{0.65}CO_3$ studied by other authors [20, 18], and the yellow solid line on $FeCO_3$. The data from the mixed-spin region reported by Fu et al. [18] was omitted for clarity.

spin phase. In this study we focused on the pure-spin phases of $Mg_{1-x}Fe_xCO_3$ and showed that increasing iron content leads to larger differences in sound velocities and velocity anisotropies after the spin transition. Thus iron-rich regions in the deep mantle might show even higher seismic contrast between $Mg_{1-x}Fe_xCO_3$ and other minerals.

In order to quantitatively test the geophysical significance of our results we have investigated the influence of $Mg_{1-x}Fe_xCO_3$ on the velocity profiles in the Earth's lower mantle. We performed the calculations using the BurnMan package [33] employing a model of pyrolitic mantle as given by Wang et al. (2015) [34] with 80 % bridgmanite (5 % $FeAlO_3$) and 20 % ferropericlase (18 % FeO) and considered varying amounts of $Mg_{1-x}Fe_xCO_3$. Data for bridgmanite and ferropericlase was taken from Stixrude & Lithgow-Bertelloni (2005) [35], and all compositions are given in mol %. We have investigated the velocities in the upper part of the lower mantle in the pressure range up to 60 GPa, which

according to the PREM model [36], corresponds to a depth region of 700-1450 km. We have included the temperature effect on $Mg_{1-x}Fe_xCO_3$ taking the temperature derivative of elastic tensor from Yang et al. (2014) [19] and density correction from Dorogokupets (2007) [37].

The spin transition in $FeCO_3$ gives a visible velocity contrast (at least 1 %) if at least 4 % of pure $FeCO_3$ is present in a pyrolitic mantle. In that case the shear velocity of the high-spin carbonated pyrolite is 2 % lower and for low spin $FeCO_3$ less than 1 % lower than that of non-carbonated pyrolite. A similar effect is visible for compressional waves if 10 % of $FeCO_3$ is present, where in the high-spin region velocity is lower by 3%, and in low-spin by 2%. However $Mg_{0.85}Fe_{0.15}CO_3$ is proposed to be the composition of lower mantle carbonate. As discussed in section 4.3, this composition shows small velocity contrasts over the spin transition for pure $Mg_{0.85}Fe_{0.15}CO_3$, which is negligible in a lower mantle pyrolite assemblage. Our calculations show that an addition of 10% of $Mg_{0.85}Fe_{0.15}CO_3$ would lower the shear velocity of carbonated pyrolite by 1 %, and the addition of 9 % $Mg_{0.85}Fe_{0.15}CO_3$ would lower the compressional velocity by 1 %. The calculations do not include the effect of velocity anisotropy, which could be an additional discriminant for the presence of carbonates in the lower mantle. The high anisotropy of carbonates mentioned by Sanchez-Valle et al. (2011) [20] is confirmed in this study up to 60 GPa. After the spin transition AV_p decreases with pressure, while AV_s increases up to 49% at 60 GPa. The extrapolation of the current dataset to deeper parts of the lower mantle is ambigous, because of the non-linear behaviour of C_{11} and C_{44} of $MgCO_3$, and beyond the scope of this study.

5. Conclusions

We experimentally obtained C_{33} and C_{44} elastic stiffness moduli of $FeCO_3$ across the pressure-induced spin transition. These data confirm the results obtained by DFT calculations, where the latter provided all tensor components up to 60 GPa. We have also calculated the full elastic tensor of $MgCO_3$ up to 60

GPa and compared our results to the experimental data [19]. Our calculations are in good agreement with experiments with the exception of the systematically lower value of the C_{12} modulus.

We have investigated the influence of the composition of $Mg_{1-x}Fe_xCO_3$ carbonates on their high pressure elastic properties by comparing the results of our calculations to literature data on $Mg_{0.35}Fe_{0.65}CO_3$. We observed an increase of both compressional and shear velocity after the spin transition.

We employed a mineral physics model of the upper part of the lower mantle and investigated the influence of $Mg_{1-x}Fe_xCO_3$ on a pyrolitic composition. We observed that the presence of $Mg_{1-x}Fe_xCO_3$ changes the shear velocity more than the compressional velocity. At least 3 % of $FeCO_3$ is needed to observe a shear velocity contrast of more than 1% due to the spin transition, and 8 % of $Mg_{0.85}Fe_{0.15}CO_3$ is needed to observe a velocity contrast of more than 1% between carbonated and non-carbonated pyrolite under lower mantle conditions.

Values of C_{ij}, velocity and velocity anisotropies for $Mg_{1-x}Fe_xCO_3$ at high pressures can be found in the supplementary dataset.

Acknowledgments

We thank Eiken Haussühl for determining the orientation of the crystals within the DAC, and Jeroen Jacobs and Lkhamsuren Bayarjargal for help with preparation of DACs. This study was supported by the joint DFG-ANR project WI1232/41-1. We are also grateful for funding by the DFG in the framework of the DFG Research Unit FOR2125 "CarboPaT".

References

[1] R. M. Hazen, C. M. Schiffries, Why Deep Carbon?, in: R. Hazen, A. P. Jones, A. Baross (Eds.), Carbon in Earth, The Mineralogical Society of America, 2013, Ch. 1, pp. 1–6.

[2] K. Turekian, K. Wedepohl, Distribution of the elements in some major units of the Earth's crust, Geological Society of America Bulletin 72 (2) (1961) 175–191.

[3] R. W. Luth, Carbon and carbonates in the mantle, in: Y. Fei, C. M. Bertka, M. B. O. (Eds.), Mantle Petrology: Field Observations and High Pressure Experimentation: A Tribute to Francis R. (Joe) Boyd, Geochem. Soc. Spec. Publ., 1999, Ch. 6, pp. 297–316.

[4] C. Biellmann, P. Gillet, F. Guyot, J. Peyronneau, B. Reynard, Experimental evidence for carbonate stability in the Earth's lower mantle, Earth and Planetary Science Letters 118 (1) (1993) 31 – 41. doi:http://dx.doi.org/10.1016/0012-821X(93)90157-5.
URL http://www.sciencedirect.com/science/article/pii/0012821X93901575

[5] K. Litasov, Physicochemical conditions for melting in the Earth's mantle containing a C-O-H fluid (from experimental data), Russian Geology and Geophysics 52 (5) (2011) 475 – 492. doi:http://dx.doi.org/10.1016/j.rgg.2011.04.001.
URL http://www.sciencedirect.com/science/article/pii/S1068797111000617

[6] Y. Seto, D. Hamane, T. Nagai, K. Fujino, Fate of carbonates within oceanic plates subducted to the lower mantle, and a possible mechanism of diamond formation, Physics and Chemistry of Minerals 35 (4) (2008) 223–229. doi:10.1007/s00269-008-0215-9.
URL http://dx.doi.org/10.1007/s00269-008-0215-9

[7] A. Wang, J. D. Pasteris, H. O. Meyer, M. L. Dele-Duboi, Magnesite-bearing inclusion assemblage in natural diamond, Earth and Planetary Science Letters 141 (1) (1996) 293 – 306. doi:http://dx.doi.org/10.1016/0012-821X(96)00053-2.

URL http://www.sciencedirect.com/science/article/pii/0012821X96000532

[8] G. Fiquet, F. Guyot, M. Kunz, J. Matas, D. Andrault, M. Hanfland, Structural refinements of magnesite at very high pressure, American Minerealogist 87 (8-9) (2002) 1261–1265.

[9] M. Isshiki, T. Irifune, K. Hirose, S. Ono, Y. Ohishi, T. Watanuki, E. Nishibori, M. Takata, M. Sakata, Stability of magnesite and its high-pressure form in the lowermost mantle, Nature 427 (6969) (2004) 60–63. doi:10.1038/nature02181.
URL http://dx.doi.org/10.1038/nature02181

[10] K. D. Oh, H. Morikawa, S. Iwai, H. Aoki, The Crystal Structure of Magnesite, American Minerealogist 58 (1973) 1029–1033.

[11] B. Lavina, P. Dera, R. T. Downs, V. Prakapenka, M. Rivers, S. Sutton, M. Nicol, Siderite at lower mantle conditions and the effects of the pressure-induced spin-pairing transition, Geophysical Research Letters 36 (23), l23306. doi:10.1029/2009GL039652.
URL http://dx.doi.org/10.1029/2009GL039652

[12] A. Mattila, T. Pylkkänen, J.-P. Rueff, S. Huotari, G. Vankó, M. Hanfland, M. Lehtinen, K. Hämäläinen, Pressure induced magnetic transition in siderite $FeCO_3$ studied by X-ray emission spectroscopy, Journal of Physics: Condensed Matter 19 (38) (2007) 386206.
URL http://stacks.iop.org/0953-8984/19/i=38/a=386206

[13] B. Lavina, P. Dera, R. T. Downs, W. Yang, S. Sinogeikin, Y. Meng, G. Shen, D. Schiferl, Structure of siderite $FeCO_3$ to 56 GPa and hysteresis of its spin-pairing transition, Phys. Rev. B 82 (2010) 064110. doi:10.1103/PhysRevB.82.064110.
URL http://link.aps.org/doi/10.1103/PhysRevB.82.064110

[14] S. S. Lobanov, A. F. Goncharov, K. D. Litasov, Optical properties of siderite ($FeCO_3$) across the spin transition: Crossover to iron-rich carbonates in the lower mantle, American Mineralogist 100 (5-6) (2015) 1059–1064. arXiv:http://ammin.geoscienceworld.org/content/100/5-6/1059.full.pdf, doi:10.2138/am-2015-5053.
URL http://ammin.geoscienceworld.org/content/100/5-6/1059

[15] A. Spivak, N. Solopova, V. Cerantola, E. Bykova, E. Zakharchenko, L. Dubrovinsky, Y. Litvin, Raman study of $MgCO_3$–$FeCO_3$ carbonate solid solution at high pressures up to 55 GPa, Physics and Chemistry of Minerals 41 (8) (2014) 633–638. doi:10.1007/s00269-014-0676-y.
URL http://dx.doi.org/10.1007/s00269-014-0676-y

[16] V. Cerantola, C. McCammon, I. Kupenko, I. Kantor, C. Marini, M. Wilke, L. Ismailova, N. Solopova, A. Chumakov, S. Pascarelli, L. Dubrovinsky, High-pressure spectroscopic study of siderite ($FeCO_3$) with a focus on spin crossover, American Mineralogist 100 (11-12) (2015) 2670–2681. arXiv:http://ammin.geoscienceworld.org/content/100/11-12/2670.full.pdf, doi:10.2138/am-2015-5319.
URL http://ammin.geoscienceworld.org/content/100/11-12/2670

[17] J. Müller, S. Speziale, I. Efthimiopoulos, S. Jahn, M. Koch-Müller, Raman spectroscopy of siderite at high pressure: Evidence for a sharp spin transition, American Mineralogist 101 (12) (2016) 2638–2644. arXiv:http://ammin.geoscienceworld.org/content/101/12/2638.full.pdf, doi:10.2138/am-2016-5708.
URL http://ammin.geoscienceworld.org/content/101/12/2638

[18] S. Fu, J. Yang, J.-F. Lin, Abnormal elasticity of single-crystal Magnesiosiderite across the spin sransition in Earth's lower mantle, Phys. Rev. Lett. 118 (2017) 036402. doi:10.1103/PhysRevLett.118.036402.
URL http://link.aps.org/doi/10.1103/PhysRevLett.118.036402

[19] J. Yang, Z. Mao, J.-F. Lin, V. B. Prakapenka, Single-crystal elasticity of the deep-mantle magnesite at high pressure and temperature, Earth and Planetary Science Letters 392 (2014) 292 – 299. doi:http://dx.doi.org/10.1016/j.epsl.2014.01.027.
URL http://www.sciencedirect.com/science/article/pii/S0012821X14000375

[20] C. Sanchez-Valle, S. Ghosh, A. D. Rosa, Sound velocities of ferromagnesian carbonates and the seismic detection of carbonates in eclogites and the mantle, Geophysical Research Letters 38 (24) (2011) L24315. doi:10.1029/2011GL049981.
URL http://dx.doi.org/10.1029/2011GL049981

[21] H. Shi, W. Luo, B. Johansson, R. Ahuja, First-principles calculations of the electronic structure and pressure-induced magnetic transition in siderite FeCO3, Phys. Rev. B 78 (2008) 155119. doi:10.1103/PhysRevB.78.155119.
URL http://link.aps.org/doi/10.1103/PhysRevB.78.155119

[22] H. Hsu, S.-C. Huang, Spin crossover and hyperfine interactions of iron in (Mg,Fe)CO_3 ferromagnesite, Physical Review B 94 (6) (2016) 060404.

[23] J. Liu, J.-F. Lin, Z. Mao, V. B. Prakapenka, Thermal equation of state and spin transition of magnesiosiderite at high pressure and temperature, American Mineralogist 99 (1) (2014) 84–93. doi:10.2138/am.2014.4553.

[24] P.-F. Chen, L.-Y. Chiao, P.-H. Huang, Y.-J. Yang, L.-G. Liu, Elasticity of magnesite and dolomite from a genetic algorithm for inverting Brillouin spectroscopy measurements, Physics of the Earth and Planetary Interiors 155 (1) (2006) 73–86.

[25] A. G. Every, A. K. McCurdy, Table 3. Cubic system. Elements, Springer Berlin Heidelberg, Berlin, Heidelberg, 1992, pp. 11–17. doi:10.1007/10046537-8.
URL http://dx.doi.org/10.1007/10046537_8

[26] B. M. French, Stability relations of siderite ($FeCO_3$) in the system Fe-C-O, American Journal of Science 271 (1) (1971) 37–78. arXiv:http://www.ajsonline.org/content/271/1/37.full.pdf+html, doi:10.2475/ajs.271.1.37.
URL http://www.ajsonline.org/content/271/1/37.abstract

[27] J. F. Nye, Physical properties of crystals: their representation by tensors and matrices, Oxford university press, 1985.

[28] S. J. Clark, M. D. Segall, C. J. Pickard, P. J. Hasnip, M. I. Probert, K. Refson, M. C. Payne, First principles methods using CASTEP, Zeitschrift für Kristallographie-Crystalline Materials 220 (5/6) (2005) 567–570.

[29] J. P. Perdew, K. Burke, M. Ernzerhof, Generalized Gradient Approximation Made Simple, Phys. Rev. Lett. 77 (1996) 3865–3868. doi:10.1103/PhysRevLett.77.3865.
URL http://link.aps.org/doi/10.1103/PhysRevLett.77.3865

[30] H. J. Monkhorst, J. D. Pack, Special points for Brillouin-zone integrations, Phys. Rev. B 13 (1976) 5188–5192. doi:10.1103/PhysRevB.13.5188.
URL http://link.aps.org/doi/10.1103/PhysRevB.13.5188

[31] D. Mainprice, G. Barruol, W. B. IsmaL, The Seismic Anisotropy of the Earth's Mantle: from Single Crystal to Polycrystal, American Geophysical Union, 2013, pp. 237–264. doi:10.1029/GM117p0237.
URL http://dx.doi.org/10.1029/GM117p0237

[32] R. Dasgupta, M. M. Hirschmann, A. C. Withers, Deep global cycling of carbon constrained by the solidus of anhydrous, carbonated eclogite under upper mantle conditions, Earth and Planetary Science Letters 227 (12) (2004) 73 – 85. doi:http://dx.doi.org/10.1016/j.epsl.2004.08.004.
URL http://www.sciencedirect.com/science/article/pii/S0012821X04004820

[33] S. Cottaar, T. Heister, I. Rose, C. Unterborn, Burnman: A lower mantle mineral physics toolkit, Geochemistry, Geophysics, Geosystems 15 (4) (2014) 1164–1179. doi:10.1002/2013GC005122.
URL http://dx.doi.org/10.1002/2013GC005122

[34] X. Wang, T. Tsuchiya, A. Hase, Computational support for a pyrolitic lower mantle containing ferric iron, Nature Geosci 8 (7) (2015) 556–559, letter.
URL http://dx.doi.org/10.1038/ngeo2458

[35] L. Stixrude, C. Lithgow-Bertelloni, Thermodynamics of mantle minerals i. physical properties, Geophysical Journal International 162 (2) (2005) 610–632. doi:10.1111/j.1365-246X.2005.02642.x.
URL http://dx.doi.org/10.1111/j.1365-246X.2005.02642.x

[36] A. M. Dziewonski, D. L. Anderson, Preliminary reference earth model, Physics of the earth and planetary interiors 25 (4) (1981) 297–356.

[37] P. I. Dorogokupets, Equation of state of magnesite for the conditions of the earth's lower mantle, Geochemistry International 45 (6) (2007) 561–568. doi:10.1134/S0016702907060043.
URL http://dx.doi.org/10.1134/S0016702907060043